A Tight-Binding Method for Predicting Magnetic Ordering in Gd-Containing Solids: Application to GdB_2C_2

Lindsay E. Roy and Timothy Hughbanks*

Department of Chemistry, Texas A&M University, P.O. Box 30012, College Station, Texas 77842-3012

Received: June 30, 2006

Herein we present a method to compute d−f mediated exchange coupling in Gd-containing systems with a spin-dependent extended Hückel-tight binding (EHTB) method. EHTB parameters were chosen to exactly reproduce the spin density functional calculation (SDFT) energy gap of the $S = 45/2$ and 39/2 spin patterns for a model compound, $Gd_6CoI_{12}(OPH_3)_6$. Comparison between SDFT and EHTB results shows a good match between the spin-pattern energy distribution for the two methods. We applied our EHTB method to the solid-state compound GdB_2C_2 by considering 6 different variations in the ordering of the $4f^7$ moments. Calculations indicate that this metallic system should exhibit antiferromagnetic ordering of the $4f^7$ moments with a magnetic structure consistent with published neutron diffraction results.

Introduction

In recent years, we have shown that Spin Density Functional Theory (SDFT) is useful for studying interatomic exchange coupling in gadolinium-containing molecules and solids.[1−4] Our approach consists of calculating the relative energies of competing "spin-patterns" in order to deduce the nature of coupling in both discrete polynuclear and extended structures. Unfortunately, this spin pattern approach can become difficult when using SDFT on compounds with extended structures that are metallic conductors. Therefore, we developed other means of describing the possible spin patterns of these solids using a carefully parametrized Extended Hückel tight binding (EHTB) approach. For a qualitative description, the spin-dimer approach based on EHTB calculations has reproduced relative strengths of the spin-exchange interactions determined from first principles electronic structure calculations for a variety of magnetic transition metal oxides.[5−10] To test our method, we studied benchmark systems for which the magnetic structure of Gd-containing solids was known using neutron diffraction techniques. Of the lanthanide elements, Gd poses a challenge because natural Gd is almost opaque to neutrons due to the high absorption cross sections of ^{155}Gd and ^{157}Gd.[11] However, it is possible to obtain magnetic structures for Gd-containing solids using compounds isotopically enriched with ^{158}Gd or ^{160}Gd.[12−15] The use of new powder neutron diffractometers[16,17] and/or hot neutrons ($\lambda = 0.58$ Å), for which the relevant absorption cross-sections are considerably smaller,[18−22] helps to alleviate difficulties posed by these heavy neutron absorbers. Mössbauer studies probing the ^{155}Gd isotope can also yield information concerning magnetic structures.[23,24]

In this paper we present a spin-dependent EHTB method for predicting magnetic structures in Gd-containing solids and apply the method to the magnetic ordering in GdB_2C_2, a compound in which B/C atomic ordering has also been of long-standing interest.

Computational Details

Electronic structure calculations for YB_2C_2 were performed by using density functional theory with the Becke exchange functional and Lee−Yang−Parr correlation functional (BLYP).[25,26] All density functional calculations presented here were performed with the DMol^3 program from the Materials Studio suite of programs. The double numerical basis including d-polarization functions, DND, was employed in DMol^3 calculations for all atoms. Ruiz et al. recently showed that for transition-metal complexes, numerical basis sets are accurate and reliable alternatives to Gaussian basis functions.[27] For yttrium, a small frozen-core (1s2s2p3s3p3d) effective potential was used. All calculations included scalar relativistic effects and open-shell configurations. Because there are no fractional coordinates obtained from the neutron diffraction experiment to distinguish between the boron and carbon positions for YB_2C_2 or GdB_2C_2, we used lattice parameters and fractional coordinates from TbB_2C_2.[16,28] The criterion for the energy convergence in DFT calculations was set at 10^{-6} au. Band calculations were carried out with a mesh of 405 *k*-points throughout the Brillouin zone (BZ) to obtain density-of-states (DOS) and band structure plots of high resolution. DOS plots were generated with Cerius2 and band dispersion plots were generated with the Viewkel routine from YAeHMOP.[29,30]

EHTB calculations were carried out with the program YAeHMOP on YB_2C_2 and "GdB_2C_2" (simulating (5d/6s)-f spin polarization in GdB_2C_2, using a YB_2C_2 model to be described below). The exponents (ζ) and valence shell ionization potentials (H_{ii} in eV) are listed in the Appendix. Double-ζ Slater-type orbitals were used to represent Y 4d atomic orbitals. The band dispersion and DOS diagrams were generated with the Viewkel routine.

In these calculations, where energy differences are small, care must be exercised in the use of *k*-point meshes for band structure calculations. For GdB_2C_2 systems with a "small" tetragonal magnetic cell (i.e., for the observed antiferromagnetic spin pattern and for the ferromagnetic calculations), we used a 936 *k*-point mesh in the irreducible wedge of the BZ. *k*-points meshes in supercells were chosen such that they were *consistent* with this mesh (468 *k*-points for the tetragonal $1 \times 1 \times 2$ supercell, 432 *k*-points for the orthorhombic $2 \times 2 \times 1$ supercell). In this context, "consistent" means that the supercell *k*-points map exactly on to the subcell *k*-points and therefore energies of the small-cell spin patterns scale exactly (with

* To whom correspondence should be addressed. E-mail: trh@mail.chem.tamu.edu.

10.1021/jp064124v CCC: $33.50
Published on Web 09/20/2006

TABLE 1: 4f−5d and 4f−6s Exchange for $4f^7$ Ln Species[31] [$\Delta_{f-d} = E(^9D) - E(^7D)$; $\Delta_{f-s} = E(^9S) - E(^7S)$]

system (config)	Δ_{f-d} (eV)	system (config)	Δ_{f-s} (eV)
Gd ($4f^75d^16s^2$)	0.793	Eu^+ ($4f^76s^1$)	0.207
Eu^+ ($4f^75d^1$)	0.806	Gd^{2+} ($4f^76s^1$)	0.292
Gd^{2+} ($4f^75d^1$)	1.070	Tb^{3+} ($4f^76s^1$)	0.325
Tb^{3+} ($4f^75d^1$)	1.271		

volume) when recomputed in the supercells. We performed test calculations with a smaller mesh (550 *k*-points in the irreducible wedge of the small tetragonal cell) and the spin-pattern energy differences were within 28 cm^{-1} of the energy differences reported here; 28 cm^{-1} may therefore be regarded as a pessimistic upper bound on the precision with which the spin-pattern energies given in Figure 8 are computed.

4f−5d/6s Exchange Simulation. Intraatomic exchange between 4f electrons and valence 5d/6s electrons in the lanthanide elements can be substantial. Such exchange is manifested in a particularly simple way in $4f^7$ Ln systems because there is no orbital contribution to the f-electron magnetic moment and f-shell electron density is spherical. The effects of 4f−5d and 4f−6s exchange are readily identified in spectra of atoms/ions with $4f^75d^16s^2$ or $4f^75d^1$ and $4f^76s^1$ configurations, data for which are given in Table 1 (see also Figures 1 and 2). The table reveals two important trends: (i) the 4f-5d exchange interaction is about four times larger than the 4f-6s exchange interaction because the 5d electrons penetrate the region of the atomic core where the f-electrons reside to a much greater extent than the 6s electrons, and (ii) in more highly charged species, the valence 5d/6s orbitals become successively more contracted and the exchange interactions increase.

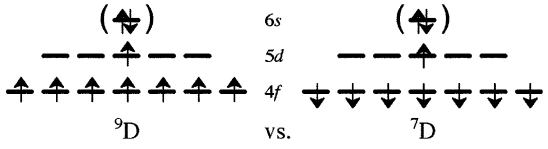

Figure 1. A spin-flip of the 4f electrons is the origin of the Δ_{f-d} promotion energy.

Because the 4f electrons in Ln atoms/ions reside in highly contracted orbitals, the most important effects of exchange arising from open f-shell atoms in molecules and solids can be understood as a perturbation of the electronic structure that one would otherwise calculate by accounting for the average spin-independent screening effect of the 4f electrons. Thus, we have found that we can interpret the magnetic exchange coupling between Gd centers in molecules calculated by use of SDFT calculations by postulating a zeroth-order spin-free system (most closely approximated in reality by Y-, La-, and Lu-containing congeners) and "turning on" the 4f-5d and 4f-6s exchange as a perturbation.[1−4] This interpretation of the SDFT calculations reveals the physical origin of such exchange coupling: it is *valence electron* (*primarily 5d*)*-mediated exchange*.

As indicated above, we have investigated the magnetic properties of molecules and solids by means of an extension of the "broken-symmetry approach",[32,33] in which we have used single-determinantal SDFT calculations to infer intraatomic exchange coupling parameters that arise from d-electron mediated f−f exchange on Gd compounds and solids.[1−4] In this approach, we calculate the energies (expectation values) of various "spin-patterns" associated with single-determinants—from the results of these calculations, one may calculate pairwise exchange parameters for that system *if* a pairwise-exchange Hamiltonian (Ising or Heisenberg) is appropriate (and in metal−metal bonded systems it usually is not). Although this approach is, in principle, applicable to any Gd-containing compound, in intermetallics with one or more partially occupied band(s), we experience severe practical difficulties in getting calculations to converge for all but ferromagnetically ordered magnetic structures. We have therefore constructed an EHTB scheme where the effects of 4f−5d and 4f−6s exchange interactions are effectively simulated.

The scheme is as follows:

(1) Using DFT, we calculate the electronic structure of a nonmagnetic congener of the Gd-containing compound in question; we do this by treating the yttrium analogue.

(2) We then carry out a calculation on the same system using extended Hückel theory, adjusting the EHTB parameters (atomic orbital energies, H_{ii}'s, and orbital exponents, ζ's) if necessary, to match the orbital energies from the EHTB calculation with the Kohn−Sham energies from the DFT calculation. In general, this requires only modest changes in the EHTB parameters since the EHTB method usually provides a good independent electron description of intermetallic compounds.

(3) We then introduce the 4f−5d and 4f−6s exchange splittings in the EHTB parameters for the Gd 5d and 6s orbitals. This was accomplished by assuming that we can carry out two EHTB calculations, one for up-spin valence electrons and one for down-spin valence electrons. Since, to an excellent approximation, the $4f^7$ moments exert their effect *locally* (as an on-site perturbation), we assume that their exchange effect can be accounted for by splitting the H_{ii} parameters from step 2 as indicated in Figure 2: orbital energies of electrons of a given spin in 5d and 6s orbitals on a Gd atom with a(n) (un)like-spin $4f^7$ moment are (de)stabilized by $^1/_2[E(^7D) - E(^9D)]$ and $^1/_2[E(^7S) - E(^9S)]$, respectively. The orbital energies are therefore split by a value of the same magnitude as the splitting found in $4f^75d^16s^2$ or $4f^75d^1$ and $4f^76s^1$ atomic systems (see below for more detail).

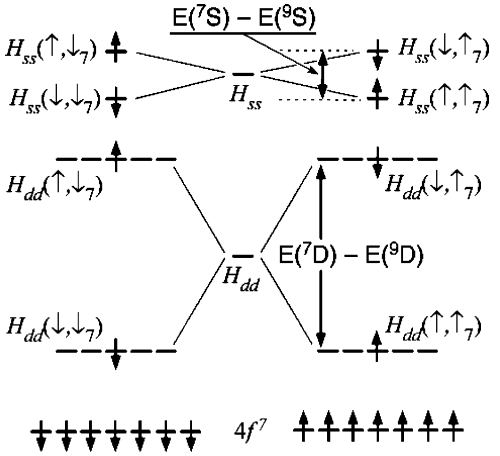

Figure 2. Spin-dependent orbital energies are used to simulate the highly local effects of 4f−5d and 4f−6s exchange splittings; $H_{ii}(\uparrow,\uparrow_7)$ and $H_{ii}(\downarrow,\downarrow_7)$ are the 5d/6s orbital energies for electrons in Gd 5d/6s orbitals with the same spin as the 4f electrons, $H_{ii}(\uparrow,\downarrow_7)$ and $H_{ii}(\downarrow,\uparrow_7)$ are the 5d/6s orbital energies for electrons in Gd 5d/6s orbitals with the opposite spin as the 4f electrons.

(4) In solid-state intermetallics, the Fermi levels of the two EHTB calculations are set equal and chosen such that the two spin populations sum to yield the correct total valence electron count.

A few comments on this procedure are in order. First of all, the actual spin-dependent parameters, $H_{dd}(\uparrow,\uparrow_7) = H_{dd}(\downarrow,\downarrow_7)$, $H_{ss}(\uparrow,\uparrow_7) = H_{ss}(\downarrow,\downarrow_7)$, $H_{dd}(\uparrow,\downarrow_7) = H_{dd}(\downarrow,\uparrow_7)$, and $H_{ss}(\uparrow,\downarrow_7) =$

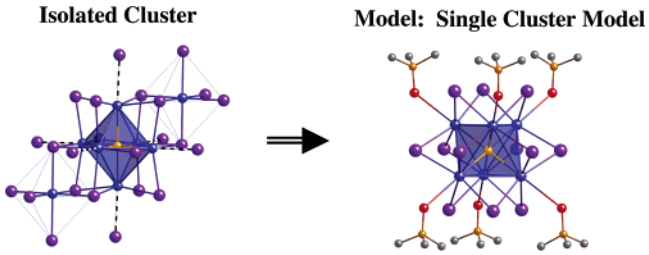

Figure 3. Relationship between the single cluster model and the parent $Gd[Gd_6ZI_{12}]$ structure.

$H_{ss}(\downarrow,\uparrow_7)$ that should be used have not yet been specified. In fact, any reasonably consistent choice would likely suffice. For example, we might have chosen $H_{dd}(\uparrow,\downarrow_7) - H_{dd}(\uparrow,\uparrow_7) = E(^7D) - E(^9D)$ and $H_{ss}(\uparrow,\downarrow_7) - H_{ss}(\uparrow,\uparrow_7) = E(^7S) - E(^9S)$ using values for either the Gd^{2+} or Eu^+ ions and either pair of parameters would probably reproduce all the trends we discuss in the examples to be presented below. Instead, we used parameters that reproduce the exact SDFT energy gap of the $S = 45/2$ and 39/2 spin patterns for a model compound, $Gd_6CoI_{12}(OPH_3)_6$, we recently published in a paper studying Gd−Gd exchange in hexanuclear clusters—see the molecular example below.[4] As an indication of the transferability of these parameters, we note that these spin-dependent EHTB model calculations closely reproduce the results of a SDFT ferromagnetic calculation on Gd_2Cl_3, in that the splittings between the ↑- and ↓-spin bands are very nearly equal in both calculations. Second, we note that it is not actually necessary to perform separate ↑- and ↓-spin calculations for an antiferromagnetic 4f-spin-pattern where all the Gd atoms are crystallographically equivalent (and the magnetic structure is equivalent to its antistructure). In this case, only a single EHTB calculation is required since the ↑- and ↓-spin 5d/6s electron band structure is the same (the *local* spin 5d/6s polarizations are *not* the same, but when summed over all atoms, the ↑- and ↓-spin 5d/6s populations are the same). Finally, of course, it is not necessary to explicitly include the 4f electrons in the EHTB calculation(s) since what determines the relative energies of competing 4f-spin-patterns is the perturbation they induce in the 5d/6s valence electronic structure.

A Molecular Example. We have previously shown that DFT calculations on the model molecular system, $[Gd_6CoI_{12}](OPH_3)_6$, predict that the delocalized cluster bonding electrons are highly effective at mediating intracluster ferromagnetic exchange coupling between the Gd atom $4f^7$-moments.[4] This model mimics the nearly O_h cluster core environment found in the solid-state compounds $Gd[Gd_6ZI_{12}]$ (Z = Mn, Fe, Co) (Figure 3). The effective magnetic moments of $[Gd_6ZI_{12}]^{3-}$ (Z = Mn, Fe) clusters are significantly increased by strong exchange interactions between the unpaired electrons in the HOMO and the electrons in the 4f orbitals (at low temperatures, the susceptibility is suppressed due to intercluster coupling). Our cluster model possesses a half-filled t_{1u}^3 HOMO configuration to avoid computational complications that arise from obtaining different electronic configurations for the high-spin and broken-symmetry solution. SDFT results predict that as Gd 4f moments are successively "flipped" over, the energy increases in steps of ~1480 cm^{-1} (range:1380−1600 cm^{-1}) for each Gd moment flipped (see Figure 4).

To simulate the exchange splittings calculated by SDFT, two EHTB calculations are necessary for each of the 10 possible 4f spin patterns to account for the ↑- and ↓-spin valence electrons. The number of electrons for the two calculations is set such that there are three unpaired electrons, one in each of the t_{1u} orbitals. Some comments and figures explaining how the

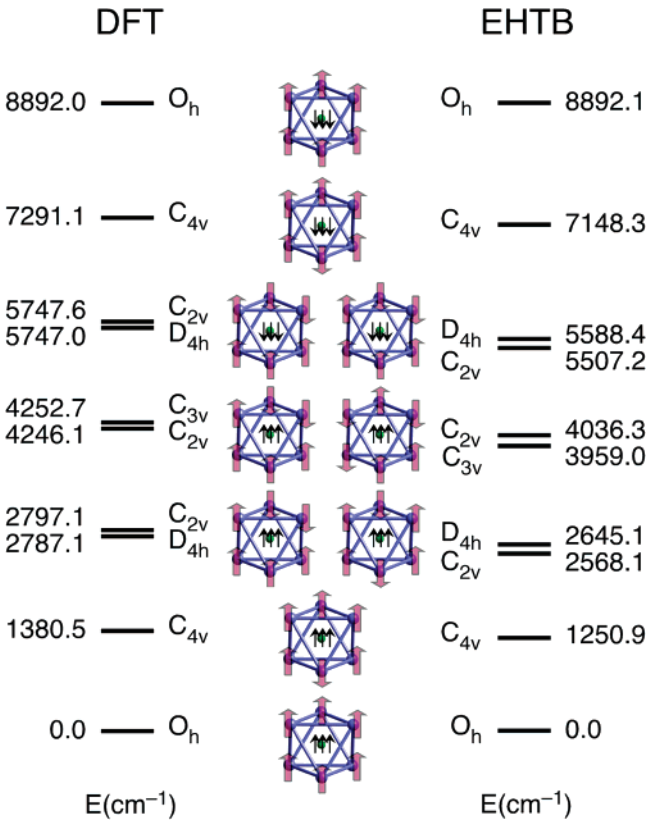

Figure 4. Comparison of DFT and EHTB results of 10 spin patterns and energies for the model $Gd_6CoI_{12}(OPH_3)_6$. The symmetries of the exchange potential are used to label the spin patterns.

energies discussed below are computed by using the EHTB model are given in the Supporting Information.

Just as we found using SDFT, the EHTB results (Figure 4) show that single cluster calculations indicate a strong preference for ferromagnetic coupling within the cluster. The energy of successive spin patterns resemble DFT results and show that the energy required to flip a 4f moment from an orientation parallel with the unpaired t_{1u} electrons to an antiparallel orientation averages ~1470 cm^{-1} per moment (range: 1250−1743 cm^{-1}). The spatial relationship between flipped moments has a relatively small effect on the calculated energies—the difference between *cis*- and *trans*- or *fac*- and *mer*- differs by ~77 cm^{-1}—but these differences are larger than those calculated using SDFT and the two approaches invert the ordering of these spin pattern "isomers". It is possible that these small differences have their origin in the fact that the H_{ij} integrals in the EHTB method depend on the magnitude of the H_{ii}'s. The magnetic coupling constant (J_{EHTB}) for the EHTB model's splitting is +134 (2) cm^{-1} (J_{SDFT} = +138.0 (0.9) cm^{-1}) using the simple spin Hamiltonian in which the Gd moments *effectively* communicate through the Co interstitial atom (1):

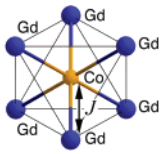

1

$$\hat{H} = -J\sum_{i=1}^{6} S_{Gd}S_{Co} \qquad S_{Gd} = \frac{7}{2};\ S_{Co} = \frac{3}{2} \qquad (1)$$

The coupling constant and inspection of Figure 4 yield the expectation that our EHTB parameters *should* yield effective exchange coupling that closely simulates SDFT calculations, since the spin-dependent EHTB parameters were chosen to

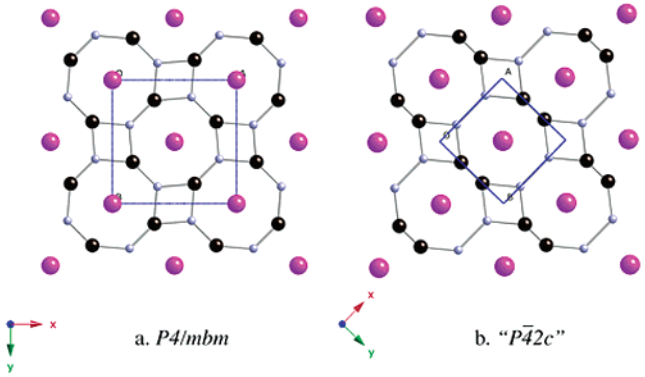

Figure 5. Alternative structural models for LnB_2C_2 (Ln = La, Ce, Pr, Nd, Tb, Dy, Ho, Er, Tm, Lu) with the unit cells shown.

exactly reproduce the SDFT energy gap of $S = 45/2$ and $S = 39/2$.

Magnetic Ordering in GdB_2C_2. LnB_2C_2 phases possess a three-dimensional structure built up by alternating the stacking of 2-D layers of Ln atoms and 4.8^2 B_2C_2 nets (in which B_2C_2 rhombi are cross-linked by B−C bonds). Viewing the structure down the *c*-axis, the Ln atom is positioned between the centers of eight-membered B_4C_4 rings. Despite the relative simplicity of this structure, two important structural characteristics of the LnB_2C_2-type have been debated in the literature. For many years, it was unclear (i) whether, as described, the B_2C_2 rhombi were cross-linked by B−C bonds or by B−B and C−C bonds (Figure 5) and (ii) whether the B/C atoms in successive layers were stacked directly or alternately in the *z*-direction (and the *c*-axis was thereby doubled).[34−37] Single-crystal X-ray diffraction studies on YB_2C_2, CaB_2C_2, and LaB_2C_2 reported B−B and C−C contacts within the eight-membered ring and a second B/C net at $z = {}^1/_2$ rotated by 90° with respect to that at $z = 0$ to give a (a, a, $2c$) tetragonal cell (Figure 5b).[36,38]

However, the results of recent neutron diffraction experiments established that these compounds possess a network structure with B−C bonds between and within the B_2C_2 rhombi and showed no doubling of the *c*-axis (Figure 5a).[28,37] The bonding connectivity in this structural model is that originally proposed by Smith, though Smith had not refined the B and C positional parameters.[35] This structure is also consistent with that predicted by Burdett et al., who used extended Hückel theory to analyze the B−C bonding arrangements in CaB_2C_2 and LaB_2C_2. In both cases, the alternating B−C bonded network structure was predicted to enjoy a large energetic advantage.[39] These predictions have been very recently borne out in a detailed DFT investigation of the structures of these compounds.[40]

Beyond these structural issues, the tetragonal rare-earth diborocarbide compounds have interesting magnetic and conducting properties.[16,41−46] The metallic conductivity is consistent with a formal electronic configuration written as $R^{3+}(B_2C_2^{2-})e^-$, where the $B_2C_2^{2-}$ sheets, like graphite and hexagonal boron nitride, possess filled π-bonding bands. The additional electron partially fills broad bands with mixed $B_2C_2(\pi^*)$-R(d) parentage. YB_2C_2 and LuB_2C_2 are superconductors with respective transition temperatures, T_c, of 3.6 and 2.4 K.[47] Other LnB_2C_2 compounds are not superconducting, but show magnetic ordering transitions below 30 K. DyB_2C_2 and HoB_2C_2 are known to undergo antiferroquadrupolar (AFQ) ordering, then below T_N, the antiferromagnetic ordering coexists with the AFQ order.[42,44,46,48,49] AFQ ordering yields supercell structures that are determined with resonant X-ray scattering and neutron diffraction techniques.[42−44,48] Among the LnB_2C_2 compounds, TbB_2C_2 is unique in that it is the only one known to exhibit field-induced AFQ ordering.[45]

Of course, the magnetic ordering in GdB_2C_2 presents the simplest computational problem; Gd lacks an orbital moment so the magnetic anisotropy is very small and it has no quadrupolar moment. Neutron diffraction experiments on a crystalline powder sample of GdB_2C_2 showed an antiferromagnetic phase transition at 47.5 K; the magnetic cell is the same as the unit cell (a, a, c), but with reduced symmetry (magnetic space group: $P4/m$).[16] The magnetic moments are antiferromagnetically ordered in the *ab* plane and are aligned along the *c*-axis.

We have examined the magnetic coupling in this system using the EHTB model described above. Hence, the electronic structure of the nonmagnetic analogue, YB_2C_2, was first considered; electronic band calculations for YB_2C_2 were performed at the semiempirical and first-principles levels of theory. Then the exchange effects exerted by the 4f moments are included as a spin-dependent perturbation to the Gd atom 5d- and 6s-orbital energies (H_{dd} and H_{ss}) in the EHTB calculations.

For this example, the tight-binding calculations are carried out as follows: (a) For a ferromagnetic spin-pattern (all up-spin Gd centers), two EHTB calculations are performed: one using parameters appropriate for up-spin 5d/6s-electrons and one for down-spin 5d/6s-electrons. The Fermi levels for the two calculations are set equal and chosen such that the total number of electrons for the system is appropriate. (b) For all the antiferromagnetic 4f-spin-patterns considered here, the Gd atoms are crystallographically equivalent (and the magnetic structures are equivalent to their antistructures), only a single EHTB calculation is required since the up- and down-spin 5d/6s electron band structure is the same. (c) For an antiferromagnetic 4f-spin-pattern where all the Gd atoms are not crystallographically equivalent, the up- and down-spin 5d/6s electron band structures are not the same and two EHTB

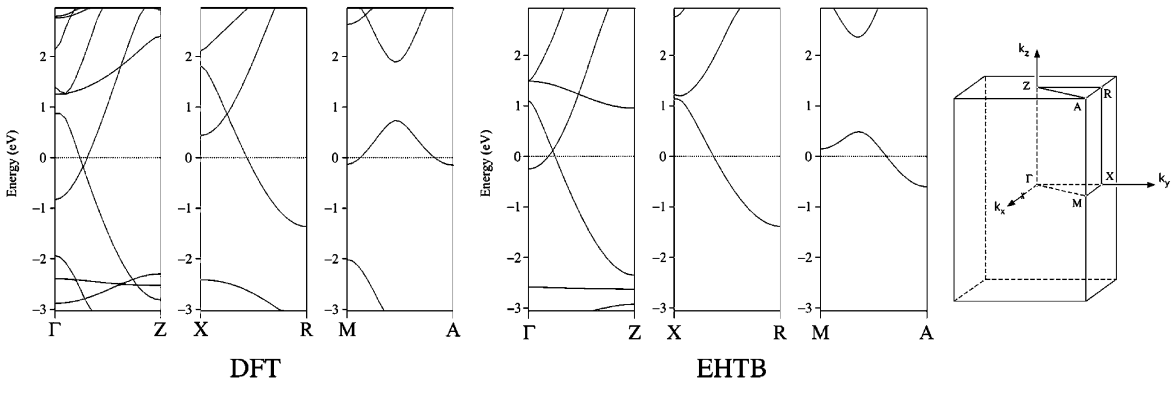

Figure 6. DFT and EHTB band structures of YB_2C_2 plotted along selected symmetry lines.

calculations must be performed, but this scenario did not occur in this case.[2]

Preliminary calculations using the standard EHTB parameters yielded good correspondence between the EHTB band structure for $B_2C_2^{2-}$ (CaB_2C_2 without Ca atoms included) and the CaB_2C_2 DFT band structure. It was therefore deemed reasonable to expect that only modest changes of the yttrium parameters would be necessary to improve the agreement between DFT and EHTB for YB_2C_2. For the bands near the Fermi level (for which a good match is crucial for success of this approach), the correspondence between the EHTB and DFT calculations is good; the borocarbide σ and π bands have approximately the same bandwidths and the conduction band begins at about the same relative energies. The calculated dispersion curves for these bands along several symmetry lines of the BZ are shown in Figure 6 for YB_2C_2 by using EHTB and DFT computations. The bands calculated by both methods "run" the same way, and except for small energy differences at the high symmetry points, the two methods look nearly identical. At the Fermi level, they exhibit dispersion of about 3.5 eV along the *c* direction (Γ−Z direction of the BZ) and 0.5 eV in the *ab* plane (X−M and R−A directions of the BZ). Throughout most of the BZ, the bands cut by the Fermi level have primarily x^2-y^2/xy character (with a π^* borocarbide admixture), but near Γ the yttrium-based band with z^2 character descends to cross the Fermi level. A comparison of Mulliken charges for YB_2C_2 from DFT and EHTB methods reveals that the EHTB charge distribution is characteristically more highly polarized, but they are in accord with the trends found in DFT.[50]

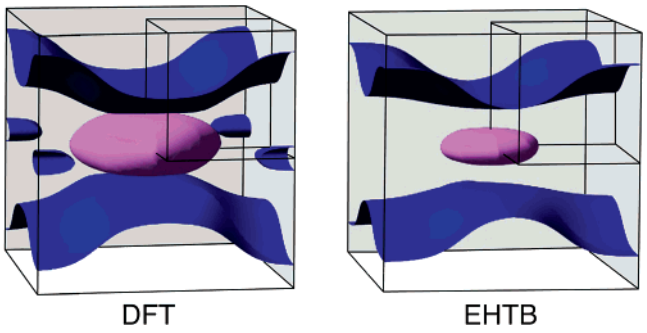

Figure 7. Fermi surface for YB_2C_2 with DFT and EHTB. Dark blue (dark gray) undulating surface: $x^2-y^2/xy/\pi^*$ band. Violet (light gray) pocket of electrons: z^2 band.

Figure 7 depicts approximate[51] Fermi surfaces (FS) as they emerge from DFT and EHTB calculations on YB_2C_2. In both cases, the large undulating surface results from a cut through the $x^2-y^2/xy/\pi^*$ band, and the pocket of electrons surrounding the Γ point results from a cut through a small segment of the z^2 band that dips below the Fermi level at the BZ center. The close similarity between the two surfaces reveals the closeness with which the parametrized EHTB calculations reproduce the DFT calculations.

In our study of the magnetic ordering in "GdB_2C_2", we performed calculations on six competing spin patterns. These include the observed antiferromagnetic ordering pattern, with a magnetic unit cell commensurate with the structural cell (*a*, *a*, *c*); a ferromagnetic pattern; and two additional spin-patterns for each of two different supercells, (*a*, *a*, 2*c*) and (2*a*, 2*a*, *c*). The calculated relative energies for the patterns are shown in Figure 8. In each case, we indicate the periodicity and space group imposed by the 4f exchange potential. The results in Figure 8 show a preference for an antiferromagnetic spin pattern corresponding to the experimentally observed spin ordering with adjacent magnetic moments parallel along the *c*-axis and antiparallel within the *ab* plane. Interestingly, the exchange potential of the four lowest energy spin-patterns is consistent with the 4/*m* symmetry in the Gd atoms, situated as they are between the B_4C_4 rings. The other spin patterns, in which the 4f spins change the translational periodicity in the *ab* plane, lie higher in energy. For these two spin patterns, the symmetry of the magnetic cell (and therefore, the exchange potential) is reduced from tetragonal to orthorhombic.

It is interesting to evaluate whether the relative energies of the spin patterns can be described in terms of three Ising coupling constants (*J*′). Six spin patterns yield five independent energy differences and these energy differences can also be expressed in terms of an expression involving Ising coupling parameters. We attempted the use of a linear least-squares fit to "determine" the three nearest neighbor magnetic coupling constants, but just as we concluded in our study of Gd_2Cl_3,[2] an Ising model is inappropriate for describing the d-electron mediated magnetic interaction between the 4f moments.

Electronic instabilities can sometimes be related to the topology of a compound's FS. If a large area of the FS can be translated by a vector **q** and superimposed on another region of the surface, then the FS is said to be "nested" by the vector **q**. Ignoring the pocket of electrons from the z^2 orbital around Γ (see Figure 7), the undulating sheets would superimpose on one another by a vector of (0.5, 0.5, 0.52) using DFT, (0.5, 0.5, 0.44) using EHTB, from the center of the lower to the edge of the upper sheet. However, the curvatures of the two sheets are different enough that the "nesting" is rather poor. The presence of the z^2 "pocket" further disrupts any potential nesting. If FS nesting *were* apparent then we might have expected to observe an antiferromagnetic spin pattern with an enlarged unit cell commensurate, or nearly commensurate, with the nesting vector. As it happens, it is difficult to rationalize a spin-pattern preference based on FS nesting.

We used our approach to determine whether the "$P\bar{4}2c$" structure type would be expected to exhibit magnetic ordering consistent with the observed neutron diffraction results. We performed calculations on four competing spin patterns which included the antiferromagnetic ordering observed in the *P*4/*mbm* structure, a ferromagnetic pattern, and two additional antiferromagnetic spin-patterns.[52] Interestingly, the wrong structure type produces the wrong magnetic ordering. The lowest spin pattern predicts antiferromagnetic alignment along the *ab* plane, the lowest pattern predicts antiferromagnetic coupling along the *z*-axis.

Concluding Remarks

Magnetic ordering in Gd-containing compounds is controlled by interatomic exchange that is mediated by the valence electrons with Gd 5d/6s character. Thus, by far the most interesting Gd-based magnetic compounds are intermetallics and other reduced compounds. We find that carefully parametrized EHTB calculations, in which bands near the Fermi level simulate those which emerge from DFT calculations (and having significant 5d/6s character), can be used to predict magnetic structures—even in structurally complex solids.

Finally, we should note that our approach is fundamentally the same as has been used to explain exchange coupling in Ln-based intermetallics for many years, i.e., RKKY coupling. 4f−5d/6s exchange was long-ago recognized to operate as a "contact" perturbation to the conduction electrons, but has not been used within a tight-binding formulation to predict magnetic ordering in compounds with complex electronic structures.

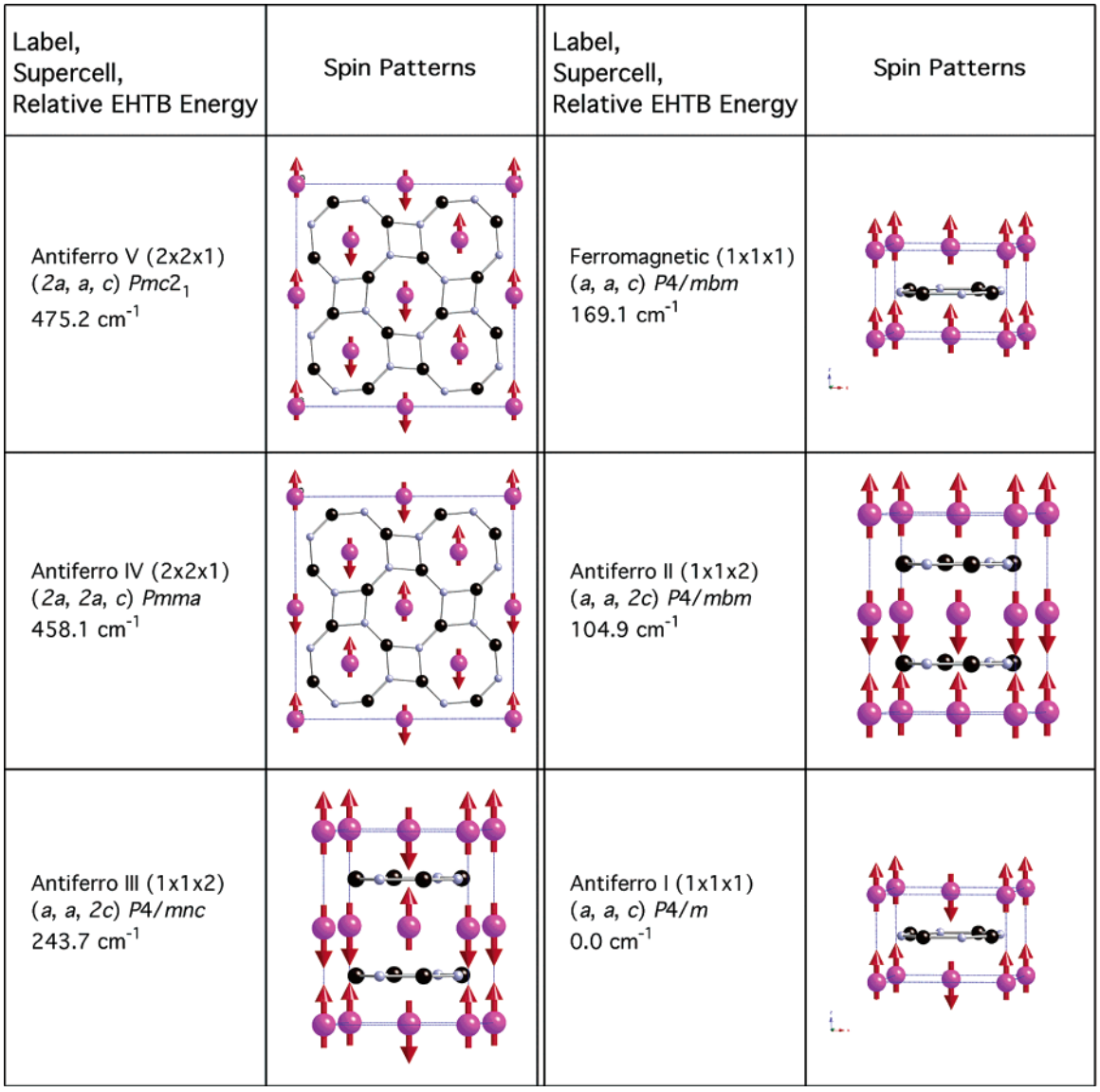

Figure 8. Proposed spin patterns for "GdB_2C_2" with *P*4/*mbm* symmetry.

We are now examining other Gd-containing intermetallics for which magnetic structures are known to further test our approach.

Acknowledgment. We wish to thank Jairo Sinova, Department of Physics, Texas A&M University and Hideya Onodera, Department of Physics, Tohoku University for their helpful discussion on quadrupole ordering. We also wish to thank Dong-Kyun (Don) Seo, Department of Chemistry, Arizona State University for helpful discussions and an advance copy of his manuscript. This work was supported by the Robert A. Welch Foundation (Grant A-1132) and the Texas Advanced Research Program (Grant No. 010366-0188-2001). We also thank the Laboratory for Molecular Simulation at Texas A&M University for computing time and other support.

Appendix

EHTB calculations were carried out with the program YAeHMOP on YB_2C_2 and "GdB_2C_2" (simulating atomic (5*d*/6*s*)-*f* exchange effects with spin-dependent H_{ii}'s given in Table 2). The exponents (ζ's) and other valence shell ionization potentials (H_{ii}'s in eV) are listed.

TABLE 2: Extended Hückel Exponents (ζ), Valence Shell Ionization Potential (H_{ii}'s in eV), and Coefficients

atom	orbital	H_{ii} (eV)	ζ_1	ζ_2	c_1	c_2
B	2s	−15.2	1.30			
	2p	−8.5	1.30			
C	2s	−21.4	1.625			
	2p	−11.4	1.625			
Y	5s	−7.02	1.74			
	5p	−4.40	1.70			
	4d	−6.80	1.40	3.60	0.8316	0.3041
"Gd^+"[a]	5s	−7.12	1.74			
	5p	−4.40	1.70			
	4d	−7.03884	1.40	3.60	0.8316	0.3041
"Gd^-"[a]	5s	−6.91	1.74			
	5p	−4.40	1.70			
	4d	−6.56116	1.40	3.60	0.8316	0.3041

[a] Gd^+ and Gd^- are used to model the spin-dependent energies of valence s and d electrons for Gd centers with spins that are respectively aligned parallel and antiparallel with the local spin direction of the 4f electrons.

Supporting Information Available: d-electron mediated exchange in hexanuclear Clusters, Mulliken charges for YB_2C_2 with DFT and EHTB, Fermi surface of YB_2C_2 with CAESAR, and proposed spin pattern for "GdB_2C_2" with "$P\bar{4}2c$" symmetry.

References and Notes

(1) Roy, L. E.; Hughbanks, T. *Mater. Res. Soc. Symp. Proc.* **2002**, *755*, 25.
(2) Roy, L.; Hughbanks, T. *J. Solid State Chem.* **2003**, *176*, 294.
(3) Roy, L. E.; Hughbanks, T. *J. Am. Chem. Soc.* **2006**, *128*, 568.
(4) Sweet, L. E.; Roy, L. E.; Meng, F.; Hughbanks, T. *J. Am. Chem. Soc.* **2006**, *128*, 10193.
(5) Koo, H.-J.; Whangbo, M.-H. *Inorg. Chem.* **2001**, *40*, 2161.
(6) Koo, H.-J.; Whangbo, M.-H.; VerNooy, P. D.; Torardi, C. C.; Marshall, W. J. *Inorg. Chem.* **2002**, *41*, 4664.
(7) Whangbo, M. H.; Koo, H. J.; Dai, D.; Jung, D. *Inorg. Chem.* **2003**, *42*, 3898.
(8) Whangbo, M.-H.; Koo, H.-J.; Dai, D. *J. Solid State Chem.* **2003**, *176*, 417.
(9) Koo, H. J.; Whangbo, M. H.; Lee, K. S. *Inorg. Chem.* **2003**, *42*, 5932.
(10) Koo, H. J.; Dai, D.; Whangbo, M. H. *Inorg. Chem.* **2005**, *44*, 4359.
(11) Rauch, H.; Zawisky, M.; Stellmach, C.; Geltenbort, P. *Phys. Rev. Lett.* **1999**, *83*, 4955.
(12) Child, H. R.; Cable, J. W. *J. Appl. Phys.* **1969**, *40*, 1003.
(13) Guillaume, M.; Fischer, P.; Roessli, B.; Allenspach, P.; Trounov, V. *Phys. C* **1994**, *235*−*240*, 1637.
(14) Champion, J. D. M.; Wills, A. S.; Fennell, T.; Bramwell, S. T.; Gardner, J. S.; Green, M. A. *Phys. Rev. B*: *Condens. Matter* **2001**, *64*, 140407/1.
(15) Matsuda, M.; Kikkawa, A.; Katsumata, K.; Ebisu, S.; Nagata, S. *J. Phys. Soc. Jpn.* **2005**, *74*, 1412.
(16) Yamaguchi, Y.; Ohoyama, K.; Yamauchi, H.; Indoh, K.; Onodera, H. *Appl. Phys. A* **2002**, *74*, S877.
(17) Kuwahara, K.; Sugiyama, S.; Iwasa, K.; Kohgi, M.; Nakamura, M.; Inamura, Y.; Arai, M.; Kunii, S. *Appl. Phys. A* **2002**, *74*, S302.
(18) Barandiaran, J. M.; Gignoux, D.; Schmitt, D.; Gomez-Sal, J. C.; Rodriguez Fernandez, J.; Chieux, P.; Schweizer, J. *J. Magn. Magn. Mater.* **1988**, *73*, 233.
(19) Bruckel, T.; Hupfeld, D.; Strempfer, J.; Caliebe, W.; Mattenberger, K.; Stunault, A.; Bernhoeft, N.; McIntyre, G. J. *Eur. Phys. J. B* **2001**, *19*, 475.
(20) Rotter, M.; Doerr, M.; Loewenhaupt, M.; Lindbaum, A.; Ziebeck, K.; Beuneu, B. *Phys. B*: *Condens. Matter* **2004**, *350*, e63.
(21) Luca, S. E.; Amara, M.; Galera, R. M.; Givord, F.; Granovsky, S.; Isnard, O.; Beneu, B. *Phys. B*: *Condens. Matter* **2004**, *350*, e39.
(22) Rotter, M.; Loewenhaupt, M.; Doerr, M.; Lindbaum, A.; Sassik, H.; Ziebeck, K.; Beuneu, B. *Phys. Rev. B*: *Condens. Matter* **2003**, *68*, 144418/1.
(23) Tomala, K.; Sanchez, J. P.; Vulliet, P.; Canfield, P. C.; Drzazga, Z.; Winiarska, A. *Phys. Rev. B*: *Condens. Matter* **1998**, *58*, 8534.
(24) Kmiec, R.; Swiatkowska, Z.; Kruk, R.; Tomala, K. *J. Magn. Magn. Mater.* **2004**, *271*, 326.
(25) Becke, A. D. *Phys. Rev. A*: *At. Mol. Opt. Phys.* **1988**, *38*, 3098.
(26) Lee, C.; Yang, W.; Parr, R. G. *Phys. Rev. B*: *Condens. Matter* **1988**, *37*, 785.
(27) Ruiz, E.; Rodriguez-Fortea, A.; Tercero, J.; Cauchy, T.; Massobrio, C. *J. Chem. Phys.* **2005**, *123*, 074102/1.
(28) Ohoyama, K.; Kaneko, K.; Indoh, K.; Yamauchi, H.; Tobo, A.; Onodera, H.; Yamaguchi, Y. *J. Phys. Soc. Jpn.* **2001**, *70*, 3291.
(29) Landrum, G. A. *YAeHMOP*: *Yet Another extended Hückel Molecular Orbital Package*, 3.0.3; 2004. Available on the web at: http://yaehmop.sourceforge.net/.
(30) Ren, J.; Liang, W.; Whangbo, M. H. *Crystal and Electronic Structure AnalyzeR Using CAESAR*, 2.0; 2002. Available on the web at: http://www.primec.com/.
(31) NIST Exchange Splitting Energies for Gd, Eu, and Tb. http://physics.nist.gov/cgi-bin/AtData/main-asd.
(32) Noodleman, L. *J. Chem. Phys.* **1981**, *74*, 5737.
(33) Noodleman, L.; Case, D. A. *Adv. Inorg. Chem.* **1992**, *38*, 423.
(34) Smith, P. K.; Gilles, P. W. *J. Inorg. Nucl. Chem.* **1967**, *29*, 375.
(35) Smith, P. K. Ph.D. Dissertation, University of Kansas, 1965.
(36) Bauer, J.; Bars, O. *Acta Crystallogr. B* **1980**, *B36*, 1540.
(37) Van Duijn, J.; Suzuki, K.; Attfield, J. P. *Angew. Chem., Int. Ed.* **2000**, *39*, 365.
(38) The space group for this proposed structure was incorrectly reported in the original paper (*P*42*c*); the appropriate space group is $P4_2/mmc$.
(39) Burdett, J. K.; Canadell, E.; Hughbanks, T. *J. Am. Chem. Soc.* **1986**, *108*, 3971.
(40) Rocquefelte, X.; Boulfelfel, S. E.; Ben Yahia, M.; Bauer, J.; Saillard, J.-Y.; Halet, J.-F. *Angew. Chem., Int. Ed.* **2005**, *44*, 7542.
(41) Sakai, T.; Adachi, G.; Shiokawa, J. *Solid State Commun.* **1981**, *40*, 445.
(42) Yamauchi, H.; Onodera, H.; Ohoyama, K.; Onimaru, T.; Kosaka, M.; Ohashi, M.; Yamaguchi, Y. *J. Phys. Soc. Jpn.* **1999**, *68*, 2057.
(43) van Duijn, J.; Attfield, J. P.; Suzuki, K. *Phys. Rev. B*: *Condens. Matter* **2000**, *62*, 6410.
(44) Hirota, K.; Oumi, N.; Matsumura, T.; Nakao, H.; Wakabayashi, Y.; Murakami, Y.; Endoh, Y. *Phys. Rev. Lett.* **2000**, *84*, 2706.
(45) Kaneko, K.; Onodera, H.; Yamauchi, H.; Sakon, T.; Motokawa, M.; Yamaguchi, Y. *Phys. Rev. B*: *Condens. Matter* **2003**, *68*, 012401/1.
(46) Yanagisawa, T.; Goto, T.; Nemoto, Y.; Watanuki, R.; Suzuki, K.; Suzuki, O.; Kido, G. *Phys. Rev. B*: *Condens. Matter* **2005**, *71*, 104416/1.
(47) Sakai, T.; Adachi, G.-Y.; Shiokawa, J. *J. Less-Common Met.* **1982**, *84*, 107.
(48) Matsumura, T.; Oumi, N.; Hirota, K.; Nakao, H.; Murakami, Y.; Wakabayashi, Y.; Arima, T.; Ishihara, S.; Endoh, Y. *Phys. Rev. B*: *Condens. Matter* **2002**, *65*, 094420/1.
(49) 4f-electron systems, with orbital as well as spin degrees of freedom, frequently show electric quadrupole ordering (cooperative orbital alignment in f-electron systems) in addition to magnetic dipole ordering at low temperatures. Electric quadrupole interactions can give rise to ferroquadrupolar (FQ) or antiferroquadrupolar (AFQ) ordering—terms which respectively describe a uniform Ln quadrupole moment alignment or as having staggered components. The magnitudes of the quadrupolar interactions and the dipolar interactions compete in determining the type of ordering that prevails at a given temperature.
(50) Mulliken charges for YB_2C_2 with DFT and EHTB can be found in the Supporting Information.
(51) The surfaces were obtained by numerical fitting of the two bands separately; they bands mix to a small extent where the bands overlap and a more accurate Fermi surface for the EHTB calculation can be obtained with the program CAESAR; see the Supporting Information.
(52) Calculations were performed using the same procedure as outlined in the computational details and results are presented in supplementary materials.